Journal of Molecular Modeling (2018) 24: 204
https://doi.org/10.1007/s00894-018-3735-3

ORIGINAL PAPER

Electronic and optical properties of C_{24}, $C_{12}X_6Y_6$, and $X_{12}Y_{12}$ (X = B, Al and Y = N, P)

Debolina Paul[1] · Jyotirmoy Deb[1] · Barnali Bhattacharya[1] · Utpal Sarkar[1]

Received: 25 December 2017 / Accepted: 25 June 2018 / Published online: 14 July 2018

Abstract

Utilizing first-principles calculations, we studied the electronic and optical properties of C_{24}, $C_{12}X_6Y_6$, and $X_{12}Y_{12}$ fullerenes (X = B, Al; Y = N, P). These fullerenes are energetically stable, as demonstrated by their negative cohesive energies. The energy gap of C_{24} may be tuned by doping, and the $B_{12}N_{12}$ fullerene was found to have the largest energy gap. All of the fullerenes had finite optical gaps, suggesting that they are optical semiconductors, and they strongly absorb UV radiation, so they could be used in UV light protection devices. They could also be used in solar cells and LEDs due to their low reflectivities.

Keywords Fullerene C_{24} · Heterofullerenes · Electronic properties · Chemical reactivity · Optical properties

Introduction

The discovery of carbon nanostructures [1] has provided a new platform for the development of nanoscience and nanotechnology. Fullerenes, discovered by Kroto et al. [2], are allotropes of carbon. Ever since fullerenes were first reported, they have been the focus of much research, due to not only their fascinating properties but also their wide range of applications. They are employed, for example, in sensing devices [3], photovoltaic devices [4], molecular switches [5], spintronics [6], medical imaging [7], radiotherapy [8], and drug delivery [9]. Inserting a foreign atom into a fullerene influences its structural, electronic, and nonlinear optical properties [10–13]. The chemistry of the fullerenes, of which buckminsterfullerene (C_{60}) was the first to be discovered and is still the best known, has rapidly become an active area of research. C_{60} is the smallest fullerene with all five-membered rings disjoint. Likewise, C_{24} can be considered the smallest fullerene to be composed of four- and six-membered rings and to have all of its four-membered rings disjoint [14]. Fullerene structures consisting of X_nY_n (X = B, Al, Si, Zn; Y = N, P, C, S; n = 12, 24, 36) are considered to be magic fullerenes; among them, fullerene cages with n = 12 are the most stable. Hybrid semiconducting fullerenes formed from group III and V atoms, such as $B_{12}N_{12}$, $B_{12}P_{12}$, $Al_{12}N_{12}$, and $Al_{12}P_{12}$, show very good stabilities and physical properties [15]. These fullerenes are special not only because of their adsorption characteristics but also due to their low attractiveness to electrons and the wide gaps between their highest occupied molecular orbitals (HOMOs) and their lowest unoccupied molecular orbitals (LUMOs) [15]. In addition, they are used in light emitting diodes (LEDs) and fast microelectronic devices [16].

$B_{12}N_{12}$ was detected by laser desorption time-of-flight spectrometry and synthesized by Oku et al. [17, 18]. This fullerene is an excellent adsorbent and sensor for a number of molecules. Wu et al. [19] studied $(AlN)_n$ cages and reported that $Al_{12}N_{12}$ was the most energetically stable of them. Indeed, $Al_{12}N_{12}$ has received a lot of attention from researchers due to its large energy gap and special thermophysical properties [20]. It was found that fluorination can markedly decrease the large HOMO–LUMO gap of $Al_{12}N_{12}$, changing it from an intrinsic semiconductor to a p-type one [21].

Highlights
- The energy gap of C_{24} can be tuned by doping.
- $B_{12}N_{12}$ is the most stable fullerene.
- All of the fullerenes considered here are optical semiconductors.
- These fullerenes could be used in various optoelectronic devices.

Electronic supplementary material The online version of this article (https://doi.org/10.1007/s00894-018-3735-3) contains supplementary material, which is available to authorized users.

✉ Utpal Sarkar
utpalchemiitkgp@yahoo.com

[1] Department of Physics, Assam University, Silchar, Assam 788011, India

Boron phosphide (BP) is a typical refractory semiconductor [22]. There is a strong covalent bond between the B and P atoms in the BP system, and its zinc blende structure is very stable, allowing BP to be used in electronic devices operated at high temperatures. Several groups of researchers have investigated various properties of Al_nP_m clusters [23, 24]. AlP clusters are interesting to study due to their high vibrational frequencies. The vibrational progressions in their photoelectron spectra have been examined.

Investigations of systems containing C, B, and N atoms [25] and C, Al, and N atoms [26] have also been carried out. Doping $B_{12}N_{12}$ cages with C atoms has major effects on the physical and chemical properties of these cages. Carbon-based fullerenes doped with B or N (known as BCN fullerenes) are p-type or n-type semiconductors [26]. Besides their configurations and heats of formation, the electronic and chemical properties of AlN-substituted fullerenes have also been studied.

The optical properties of one- and two-dimensional carbon allotropes have been investigated by researchers in relation to their potential use in optoelectronics [27, 28]. Their optical responses can be tuned, resulting in diverse applications such as UV light protection, artificial photosynthesis, and light-to-energy conversion. However, the optical properties of fullerenes have scarcely been studied. Ching et al. [29] investigated the optical properties of C_{60} and found it to possess a low static dielectric constant with a value of 4.4. To the best of our knowledge, the optical properties of doped derivatives of C_{24} fullerene have not yet been reported. In this paper, we describe a systematic study we performed on the electronic and optical properties of C_{24}, $C_{12}X_6Y_6$, and $X_{12}Y_{12}$ fullerenes.

Computational methods

All calculations were performed within the framework of density functional theory (DFT) using the Siesta 3.2 package [30]. The generalized gradient approximation (GGA) with the Perdew–Burke–Ernzerhof (PBE) functional was adopted to treat the exchange correlation part of the density functional, and the double-zeta polarized (DZP) basis set was used along with the Troullier–Martins norm-conserving pseudopotential to obtain the minimum-energy structure as well as to explore the electronic and optical properties of fullerenes. Unrestricted spin-polarized DFT calculations were performed to examine the spin splitting in these systems. Brillouin zone sampling was achieved using an $8 \times 8 \times 8$ Monkhorst–Pack set of k points to optimize the systems, and a kinetic energy cutoff of 300 Ry was adopted.

The cohesive energy per atom (E_{coh}) was calculated using the relation

$$\frac{E_{coh} = E_{system} - [nE_C + mE_X + lE_Y]}{n + m + l,} \quad (1)$$

where E_{system} is the total energy of the fullerene and E_C, E_X, and E_Y are the total energies of the isolated C, X (= B, Al), and Y (= N, P) atoms, respectively. Here, n, m, and l are, respectively, the number of C, X, and Y atoms.

The ionization potential (I) and the electron affinity (A) of each fullerene were calculated using the formulae

$$I = E(N-1) - E(N) \quad (2)$$

$$A = E(N) - E(N+1), \quad (3)$$

where $E(N-1)$, $E(N)$, and $E(N+1)$ are the assigned energies of the $(N-1)$, N, and $(N+1)$ electron systems, respectively.

Chemical reactivity parameters such as the chemical hardness (η), chemical potential (μ), and electrophilicity index (E) were determined for each system using the following relations:

$$\eta = I - A \quad (4)$$

$$\mu = -\frac{(I+A)}{2} \quad (5)$$

$$E = \frac{\mu^2}{2\eta}, \quad (6)$$

where I is the ionization potential and A is the electron affinity of the molecular system.

The functions used to study the optical properties of the fullerenes were deduced from the frequency-dependent complex dielectric function, $\varepsilon = \varepsilon_1(\omega) + i\varepsilon_2(\omega)$, where $\varepsilon_1(\omega)$ and $\varepsilon_2(\omega)$ represent the real and imaginary parts of the dielectric function. Fermi's golden rule was used to obtain the imaginary part of the dielectric function due to interband transitions with the aid of the Kramers–Kronig relations, and the real part of the dielectric function was then derived from the imaginary part. The real and imaginary parts of the dielectric function were used to calculate other functions such as the absorption coefficient ($\alpha(\omega)$), the optical conductivity ($\sigma(\omega)$), the reflectivity ($R(\omega)$), the refractive index ($n(\omega)$), and the electron energy loss (EEL) function ($L(\omega)$) as follows:

$$\alpha(\omega) = \sqrt{2}\omega\left[\sqrt{\varepsilon_1^2(\omega) + \varepsilon_2^2(\omega)} - \varepsilon_1(\omega)\right]^{1/2} \quad (7)$$

$$\sigma(\omega) = -i\frac{\omega}{4\pi}|\varepsilon(\omega) - 1| \quad (8)$$

$$R(\omega) = \left[\frac{\sqrt{\varepsilon_1(\omega) + i\varepsilon_2(\omega)} - 1}{\sqrt{\varepsilon_1(\omega) + i\varepsilon_2(\omega)} + 1}\right]^2 \quad (9)$$

$$n(\omega) = \left[\sqrt{\varepsilon_1^2(\omega) + \varepsilon_2^2(\omega)} + \varepsilon_1(\omega)\right]^2 / \sqrt{2} \quad (10)$$

$$L(\omega) = \varepsilon_2 / \left[\varepsilon_1^2(\omega) + \varepsilon_2^2(\omega)\right], \quad (11)$$

where ω is the frequency of the electromagnetic radiation.

Results and discussion

The optimized structures of the pristine fullerene C_{24} and its doped derivatives are presented in Fig. 1. C_{24} fullerene has a stable geometry consisting of four- and six-membered rings. From the pristine C_{24}, we generated a database of two different classes each comprising four compact structures. These two classes of fullerenes derived from pristine C_{24} have the molecular formulae $C_{12}X_6Y_6$ and $X_{12}Y_{12}$, respectively. The X and Y atoms considered here are taken to be the first two members of group III (i.e., B and Al) and group V (i.e., N and P) in the periodic table, respectively. The $C_{12}X_6Y_6$ fullerenes contained 14 C–C, 4 C–X, 14 X–Y, 4 C–Y, 0 X–X, and 0 Y–Y bonds. A previous study of $C_{12}B_6N_6$ fullerenes (with four- and six-membered rings) [25] concluded that a stable structure was formed by maximizing the number of C–C and B–N bonds and minimizing the number of B–B and N–N bonds. Structures with more C–C and X–Y bonds are also

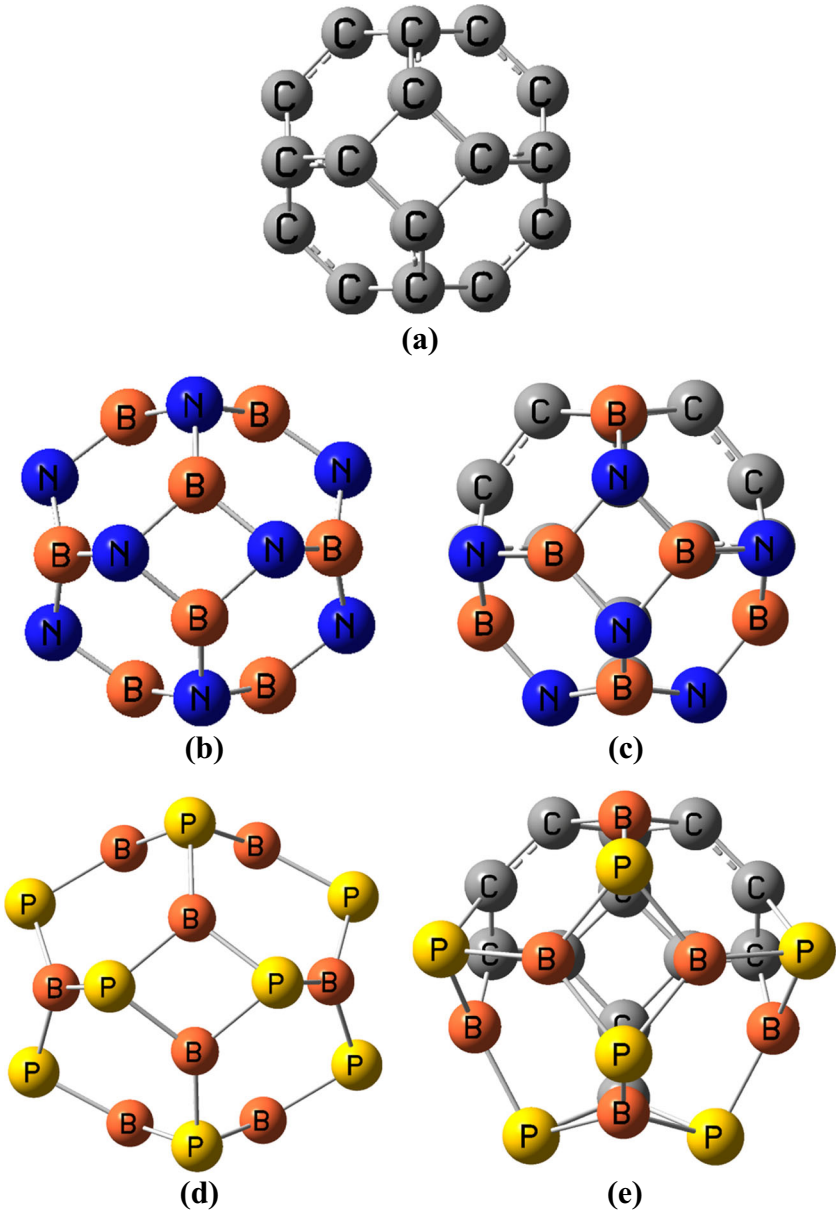

Fig. 1a–i Optimized geometries of **a** C_{24}, **b** $B_{12}N_{12}$, **c** $C_{12}B_6N_6$, **d** $B_{12}P_{12}$, **e** $C_{12}B_6P_6$, **f** $Al_{12}N_{12}$, **g** $C_{12}Al_6N_6$, **h** $Al_{12}P_{12}$, **i** $C_{12}Al_6P_6$

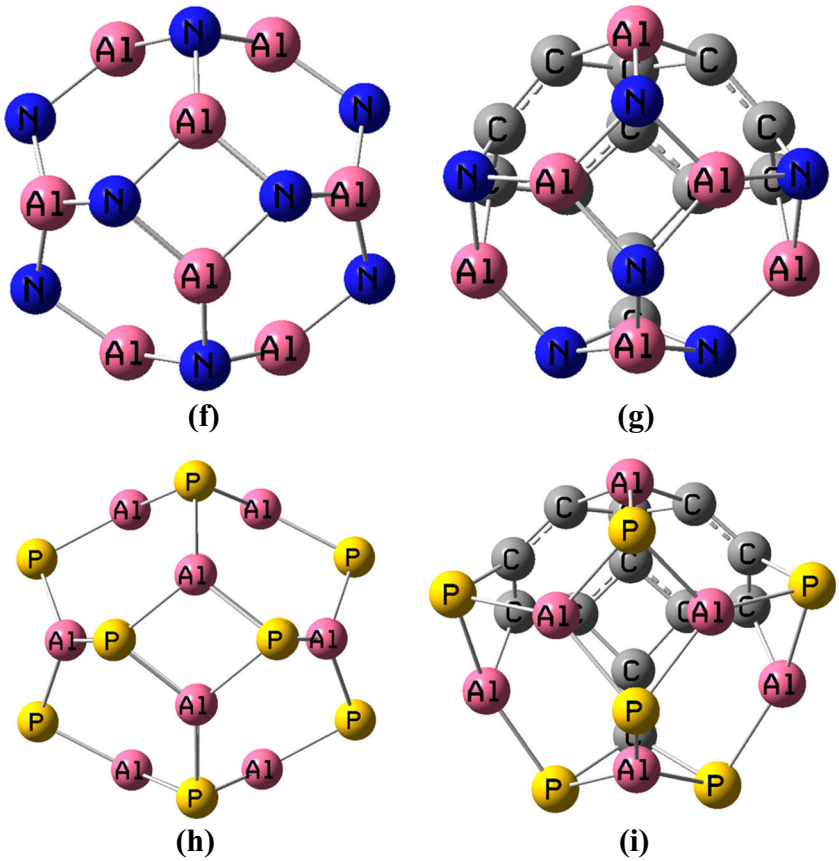

Fig. 1 (continued)

possible. However, we considered $C_{12}X_6Y_6$ systems because they yielded the largest HOMO–LUMO gaps, indicating that this configuration is more stable than the others.

Stability

In the work discussed in the present paper, the stability of fullerene molecules was explored in terms of the cohesive energy per atom. The cohesive energy per atom (E_{coh}) of each fullerene is presented in Table S1 of the "Electronic supplementary material" (ESM). Previous studies have also defined the stability of fullerenes and metal clusters using the cohesive energy/binding energy [31–35]. The cohesive energy is also important for understanding trends in the formation of fullerene molecules [33]. All of the studied fullerenes can be considered to be stable systems due to their negative cohesive energy values per atom [36]. This means that the fullerene structures do not readily collapse into their individual atoms spontaneously. The pristine fullerene C_{24} is energetically the most stable fullerene as it has the most negative cohesive energy. Introducing dopants into C_{24} reduces its stability, as observed from the more positive E_{coh} values of the heterofullerenes as compared to pristine C_{24}. The effect of doping on the stabilities of $C_{12}X_6Y_6$ and $X_{12}Y_{12}$ systems can be summarized as follows: BN doping > BP doping > AlN doping > AlP doping. The negative E_{coh} values of the fullerenes suggest that they could be synthesized via chemical vapor deposition or molecular beam epitaxy methods [37].

Electronic properties

The electronic properties of the fullerenes we examined included their HOMOs, LUMOs, and energy gaps (E_g). The stability and reactivity of any system is related to its energy gap, which is energetically equal to the difference between the HOMO and LUMO of the system. Increasing the energy gap of a system improves the stability of the system and decreases its reactivity, and vice versa. The energy gap of C_{24} was calculated to be 1.18 eV. Among the heterofullerenes, only $C_{12}Al_6N_6$ (1.08 eV) had a slightly smaller energy gap; the others had much larger energy gaps than C_{24}. For the carbon-containing heterofullerenes ($C_{12}X_6Y_6$), the energy gap was found to increase in the order $C_{12}Al_6N_6$ (1.08 eV) < $C_{12}Al_6P_6$ (1.77 eV) < $C_{12}B_6P_6$ (1.94 eV) < $C_{12}B_6N_6$ (2.19 eV). However, the energy gaps of the $X_{12}Y_{12}$ group exhibited the following trend: $Al_{12}P_{12}$ (1.99 eV) < $B_{12}P_{12}$ (2.29 eV) < $Al_{12}N_{12}$ (2.80 eV) < $B_{12}N_{12}$ (4.90 eV). Notably, in both groups ($C_{12}X_6Y_6$ and $X_{12}Y_{12}$), BN doping

significantly enhanced the stability of C_{24}, with $B_{12}N_{12}$ showing the greatest change in stability. For the $X_{12}Y_{12}$ fullerenes, the energy gaps calculated by Beheshtian et al. [38] (using the B3LYP, X3LYP, O3LYP, M05, and M06 functionals and the 6–31 G* basis set) and by Rad et al. [15] (using the B3LYP functional and the 6-31G(d,p) basis set) agree well with the trend mentioned above. Differences in values derive from differences in the level of calculation used. In our case, calculations were performed with the PBE functional and the DZP basis set. The $B_{12}N_{12}$ fullerene, which presented the largest E_g, had the greatest electrical resistivity and was therefore the most stable (least reactive) [39]. It is worth noting that for the $X_{12}Y_{12}$ fullerenes, a definite correlation was observed between E_g and the sizes of the atoms in the fullerene: larger X and Y atoms led to smaller E_g values, and their valence electrons were more likely to take part in chemical reactions and electrical conductivity. On the other hand, no such trend was observed for the $C_{12}X_6Y_6$ fullerenes, which may be due to the participation of the C atoms and the reduced proportions of X and Y atoms.

The density of states (DOS) and projected density of states (PDOS) of each fullerene are depicted in Fig. 2. According to

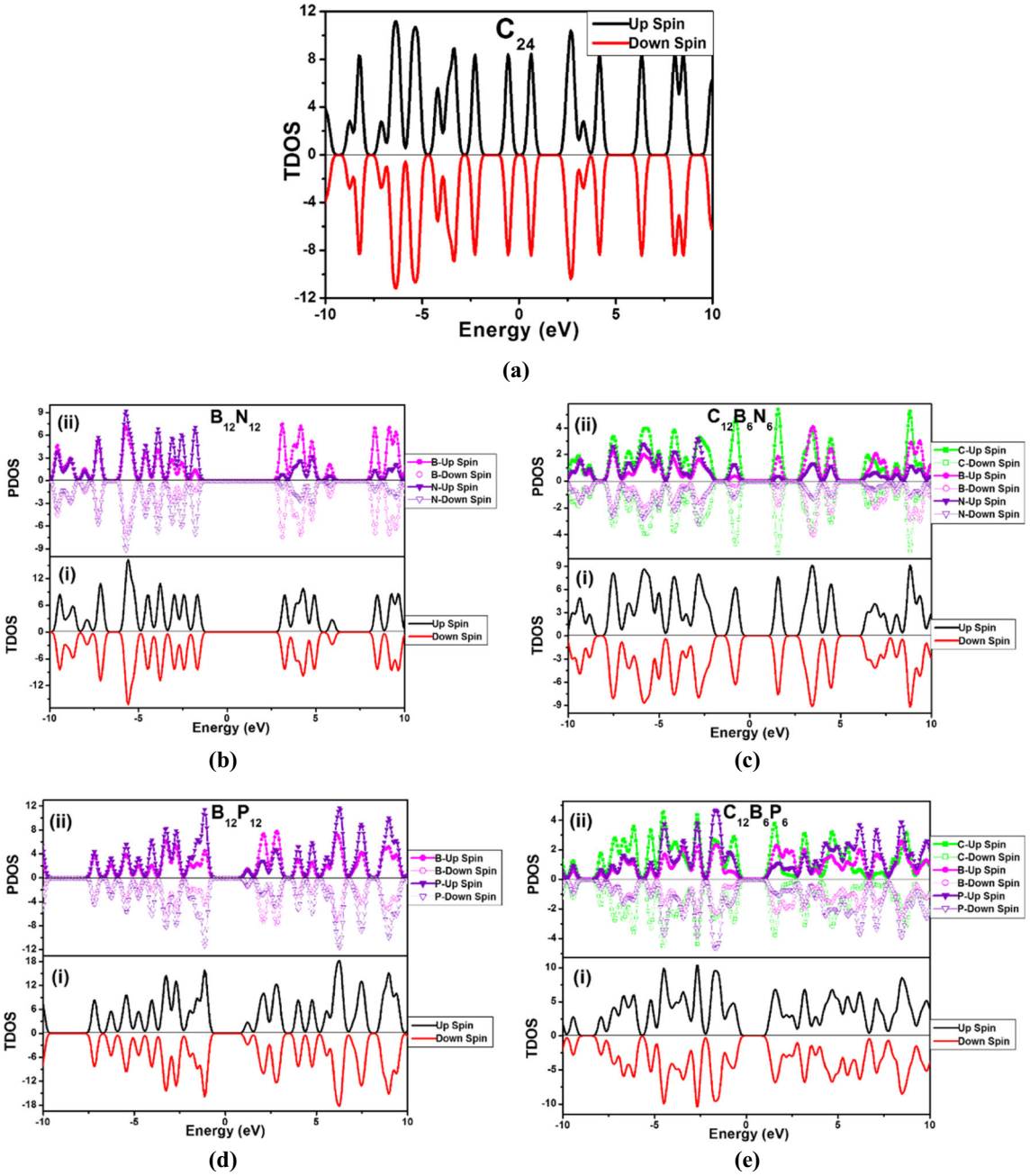

Fig. 2a–i DOS and PDOS of **a** C_{24}, **b** $B_{12}N_{12}$, **c** $C_{12}B_6N_6$, **d** $B_{12}P_{12}$, **e** $C_{12}B_6P_6$, **f** $Al_{12}N_{12}$, **g** $C_{12}Al_6N_6$, **h** $Al_{12}P_{12}$, **i** $C_{12}Al_6P_6$

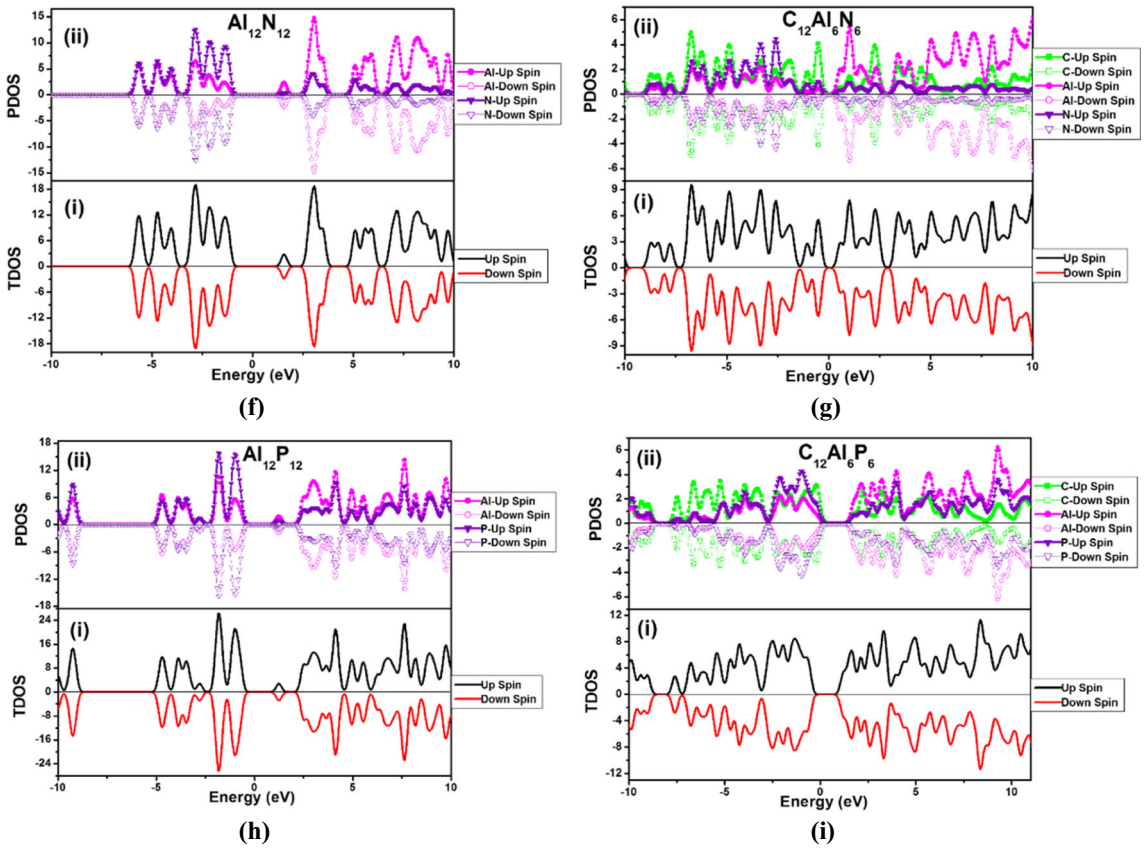

Fig. 2 (continued)

their DOSs and PDOSs, all of the fullerenes are nonmagnetic as they show no spin splitting. The pristine C_{24} has energy states spread across the specified energy range. In the case of $B_{12}N_{12}$ (Fig. 2b), the energy states of the B and N atoms contribute mostly to the LUMO and HOMO, respectively. The contribution from the B atoms gradually increases in the low-energy region of the valence band (VB) and almost overlaps with the energy states of the N atoms. However, the conduction band (CB) region is completely dominated by energy states of the B atoms, although there is a smaller contribution from the N atoms. From Fig. 2c, it is clear that the energy states in the HOMO and LUMO of $C_{12}B_6N_6$ derive primarily from the C atoms, followed by the N and B atoms. For $B_{12}P_{12}$ (Fig. 2d), we observe that energy states of both the B and the P atoms take part in the total DOS (TDOS), but the P atoms contribute more than the B atoms except for the two peaks near to the LUMO level. The energy states of the B and P atoms overlap in the LUMO, while the HOMO is dominated by states originating from P atoms. For the $C_{12}B_6P_6$ system (Fig. 2e), the contributions of the atoms to the HOMO and LUMO decrease in the following order: C atoms > P atoms > B atoms for the HOMO and C atoms > B atoms > P atoms for the LUMO. B and P both contribute significantly to the VB, but it is dominated by the contribution from the C atoms. In the CB region, the contribution from the C atoms decreases with increasing energy from 5.29 eV whereas the contributions from the P and B atoms rise. For $Al_{12}N_{12}$ (Fig. 2f), the main contributors to the HOMO and LUMO are the N and Al atoms, respectively. The amplitudes of the energy states in the HOMO are much stronger than those in the LUMO. In addition, the VB region is mostly composed of N-atom states, whereas their contribution gradually decreases in the CB region until Al-atom states dominate. In $C_{12}Al_6N_6$ (Fig. 2g), the C atoms contribute the most to the HOMO, followed by the N and Al atoms. However, in the LUMO, Al atoms provide the greatest contribution. Energy states of the Al atoms are found throughout the CB region, but they are suppressed in the VB region by energy states of the C and N atoms. $Al_{12}P_{12}$ (Fig. 2h) exhibits the same trend as $Al_{12}N_{12}$, except that the P atoms in $Al_{12}P_{12}$ play the role of the N atoms in $Al_{12}N_{12}$. Lastly, for $C_{12}Al_6P_6$ (Fig. 2i), it is clear that the energy states in the HOMO and LUMO derive from all three atomic species. In the HOMO, the C atoms make the greatest contribution, followed by the P and Al atoms, while the largest contribution to the LUMO comes from the Al atoms, followed by the C atoms and then the P atoms. Moreover, in the CB region, the Al atoms present the highest peak amplitudes, whereas in the VB region, the C atoms show the strongest peaks, except from −2.7 to −1.0 eV, where the P atoms dominate.

Chemical reactivity

The chemical reactivity parameters of these fullerenes were also examined. The chemical hardness (η) and the electrophilicity index (E) [40–44] are presented in Fig. 3, while the ionization potential (I), the electron affinity (A), and the chemical potential (μ) are shown in Fig. S1 of the ESM. These parameters are not only useful for analyzing the reactivity [45] but also for studying the reaction mechanism [46]. They can also be used to explore fullerene toxicity [47] and some excited state phenomena [48–51]. The results of our study show that the ionization potentials of $C_{12}X_6Y_6$ systems are lower than those of $X_{12}Y_{12}$ systems, which indicates that the former systems are easier to oxidize than the latter. In addition, the electron affinities of $C_{12}X_6Y_6$ fullerenes differ from those of $X_{12}Y_{12}$ fullerenes. Hence, the redox characteristics of C_{24} may be tuned by substituting X and Y atoms for C atoms, resulting in $C_{12}X_6Y_6$ heterofullerenes. Chemical hardness is a measure of chemical stability that can be investigated via the maximum hardness principle (MHP) [52–54]. Systems with large energy gaps are known to be hard and difficult to polarize since they require more energy to get them excited. On the other hand, it is easy to polarize systems with small energy gaps, which makes them more reactive than hard systems as they readily offer electrons to an acceptor [55, 56]. In the present work, the chemical hardness and the HOMO–LUMO gap were found to show the same trend for $X_{12}Y_{12}$ and $C_{12}X_6Y_6$ fullerenes, i.e., η and E_g are correlated. It is clear from Fig. 3 that $B_{12}N_{12}$ has the highest chemical hardness. Also, $B_{12}N_{12}$ has the highest ionization potential and the lowest electron affinity. The electrophilicity index is defined as the ability of a system to gain electrons, which depends not only on the chemical hardness but also on the chemical potential of the particular system (given in Eq. 6). It provides insight into the kinetic and thermodynamic properties of a system, and is also a good indicator of chemical stability, because the MHP corresponds to the minimum electrophilicity principle (MEP) [57]. Among these fullerenes, $B_{12}N_{12}$ is the least electrophilic. The correlation between the MHP and MEP indicates that harder systems are less electrophilic. Thus, $B_{12}N_{12}$ obeys both the MHP and the MEP. Furthermore, the chemical hardness is correlated with the electrophilicity index for all of these fullerenes except $C_{12}Al_6N_6$ and $Al_{12}P_{12}$. Upon switching from $C_{12}Al_6N_6$ to $Al_{12}P_{12}$, we can see that both η and E increase. To get a decrease in E, there needs to be either a negative change in μ^2 (i.e., $\Delta\mu^2$) or a negative change in η (i.e., $\Delta\eta$). Now, when we shift from $C_{12}Al_6N_6$ to $Al_{12}P_{12}$, we can see that both η and E increase (i.e., show positive changes), so we get a positive change in E, i.e., an increase in E, which leads to the discrepancy. However, as we go from $Al_{12}P_{12}$ to $C_{12}Al_6P_6$, we notice that η increases and E decreases.

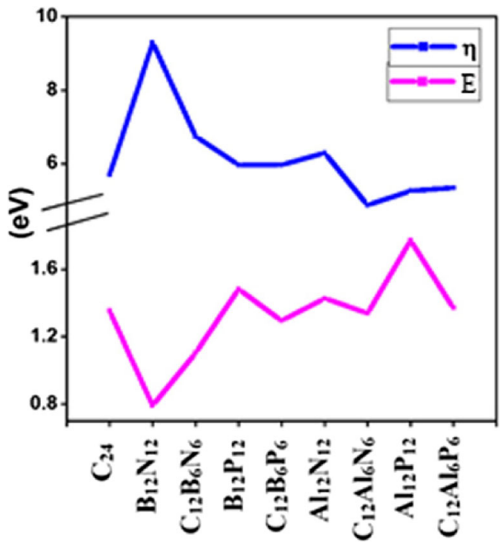

Fig. 3 Chemical hardness and electrophilicity index values of the fullerenes

Optical properties

The optical properties of the C_{24}, $C_{12}X_6Y_6$, and $X_{12}Y_{12}$ fullerenes were analyzed by introducing an average electric field. Fullerenes are isotropic molecules, so they show similar responses to an electric field applied uniformly in all directions (parallel as well as perpendicular). The optical properties for a particular system are of great importance because they carry information about the occupied and unoccupied orbitals of the electronic structure [58]. The frequency-dependent dielectric function $\varepsilon(\omega)$ is the central parameter in this respect, since it provides insight into how electromagnetic radiation influences the linear response of the system [59]. Here, $\varepsilon(\omega)$ relates to the interactions of photons with electrons. Figure 4a and b show the variations of the real part of the dielectric function for the $X_{12}Y_{12}$ and $C_{12}X_6Y_6$ fullerenes, respectively, along with C_{24}. The magnitude of the static dielectric constant for pristine C_{24} is 1.22, which decreases considerably to 1.18 for $C_{12}B_6N_6$ and increases for $C_{12}Al_6N_6$ (1.27), $C_{12}B_6P_6$ (1.34), and $C_{12}Al_6P_6$ (1.45). On the other hand, turning our attention to structures that do not have any C atoms, we can see that the magnitude of the static dielectric constant is low for $B_{12}N_{12}$ (1.11) and $Al_{12}N_{12}$ (1.20) than for C_{24}, but it is high for $B_{12}P_{12}$ (1.41) and $Al_{12}P_{12}$ (1.58). The first absorption peak in the optical spectrum represents the optical transition threshold, which corresponds to the energy gap between the highest occupied and the lowest unoccupied energy states of the fullerene, otherwise known as the optical gap. From the relevent spectra of the imaginary part of the dielectric function (Fig. 4c, d), it is apparent that the optical gaps of the C-atom-containing BN, BP, AlN, and AlP heterofullerenes increase in the order $C_{12}B_6P_6$ (2.22 eV) < $C_{12}B_6N_6$ (2.37 eV) < $C_{12}Al_6N_6$ (2.82 eV) = $C_{12}Al_6P_6$ (2.82 eV) < C_{24} (3.06 eV). For the fullerenes containing only BN, BP, AlN, and AlP, the optical

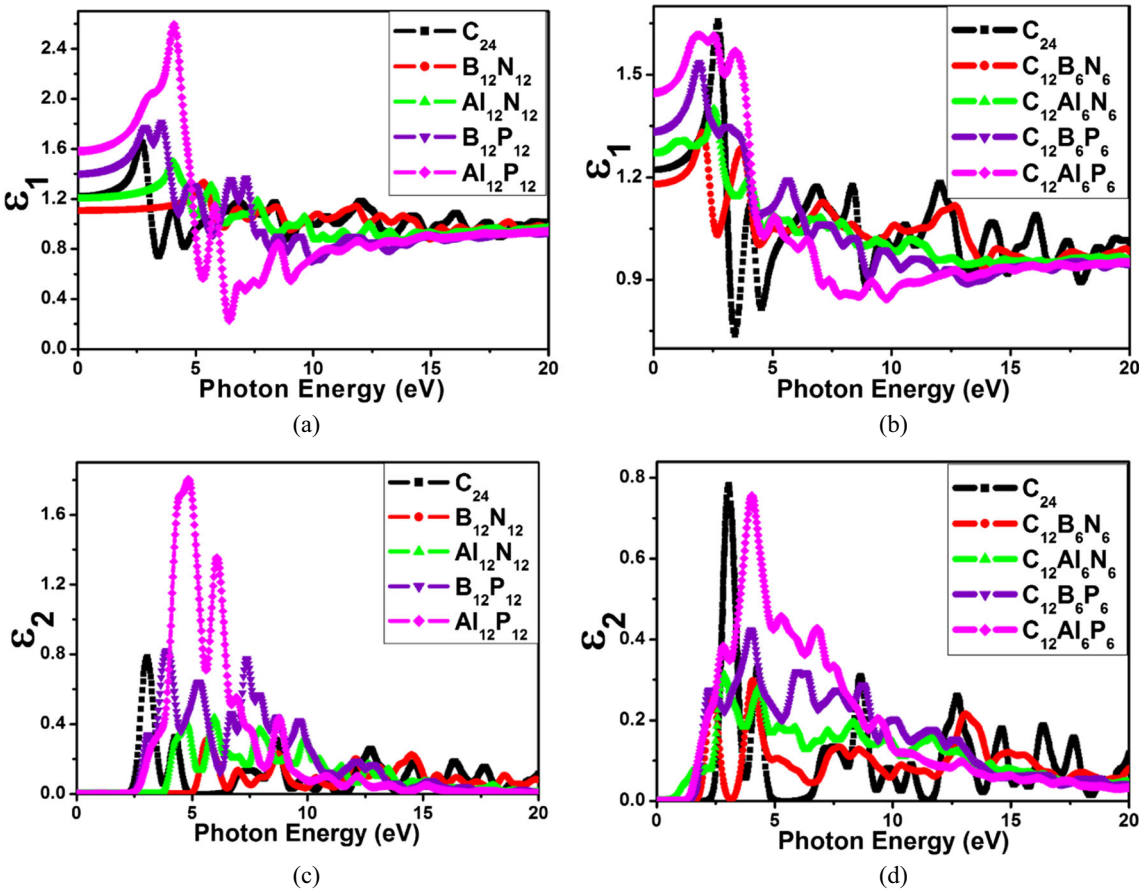

Fig. 4a–d Real (ε_1; **a**, **b**) and imaginary (ε_2; **c**, **d**) parts of the dielectric function for the $X_{12}Y_{12}$ (**a**, **c**) and $C_{12}X_6Y_6$ (**b**, **d**) fullerenes

gaps increase in the order $B_{12}P_{12}$ (3.09 eV) < $Al_{12}N_{12}$ (4.74 eV) < $Al_{12}P_{12}$ (4.83 eV) < $B_{12}N_{12}$ (5.64 eV). It should be noted that the amplitude of the absorption spectrum of the imaginary part of the dielectric function is high in the low-energy region and gradually decreases with increasing photon energy in the high-energy region. In addition, an important finding is that all of the C-containing heterofullerenes possess smaller optical gaps than their pristine C-only counterpart, while the heterofullerenes without any C atoms exhibit the highest optical gaps. The presence of an optical gap implies that these fullerenes are optical semiconductors [60, 61]. We have seen that the optical gap of pristine C_{24} can be tuned from the visible to the UV region of the electromagnetic spectrum by selecting the dopant appropriately. The first dominant peak (optical gap) of pristine fullerene occurs between the visible and UV regions. On the other hand, the first peak of each of the $C_{12}X_6Y_6$ fullerenes falls within the visible region, while that for each $X_{12}Y_{12}$ fullerene is in the UV region. Interestingly, we can see that the optical gap of C_{24} is redshifted with respect to those of $C_{12}X_6Y_6$ and blueshifted with respect to those of $X_{12}Y_{12}$ heterofullerenes. Specifically, $B_{12}N_{12}$, which has the highest optical gap, has a lower dielectric constant than C_{24} and $X_{12}Y_{12}$ fullerenes and a first high peak that is shifted towards higher energy, indicating that it has a large energy gap. Hence, it can be inferred that $B_{12}N_{12}$ could be used in short-wavelength optoelectronic devices due to its low dielectric constant and large energy gap.

The photon energy dependence of the absorption coefficient of each fullerene of interest is depicted in Fig. 5a and b. The carrier mobility of a particular system and the direction in which charge transport takes place in that system can be elucidated from its absorption spectrum. It is clear from the close-ups of the absorption spectra (insets in Fig. 5a and b) that the onset of absorption is redshifted (i.e., towards lower energies or higher wavelengths) for $C_{12}X_6Y_6$ fullerenes when compared the onset of absorption for the pristine fullerene. However, the onset of absorption for the $X_{12}Y_{12}$ fullerenes shows a different trend. It shifts to lower energy for $B_{12}P_{12}$ and $Al_{12}P_{12}$, while the other $X_{12}Y_{12}$ fullerenes present blueshifts. The absorption starts between the NIR and visible regions of the electromagnetic spectrum for pristine fullerene. Again, the onset of absorption shifts to the infrared region for the systems in which half of the C atoms in C_{24} are replaced with X and Y atoms. Among the $X_{12}Y_{12}$ fullerenes, absorption begins in the infrared region for $Al_{12}P_{12}$, between the NIR and the visible region for $B_{12}P_{12}$, in the visible region for $Al_{12}N_{12}$, and in the UV region for $B_{12}N_{12}$. Note that the onset of

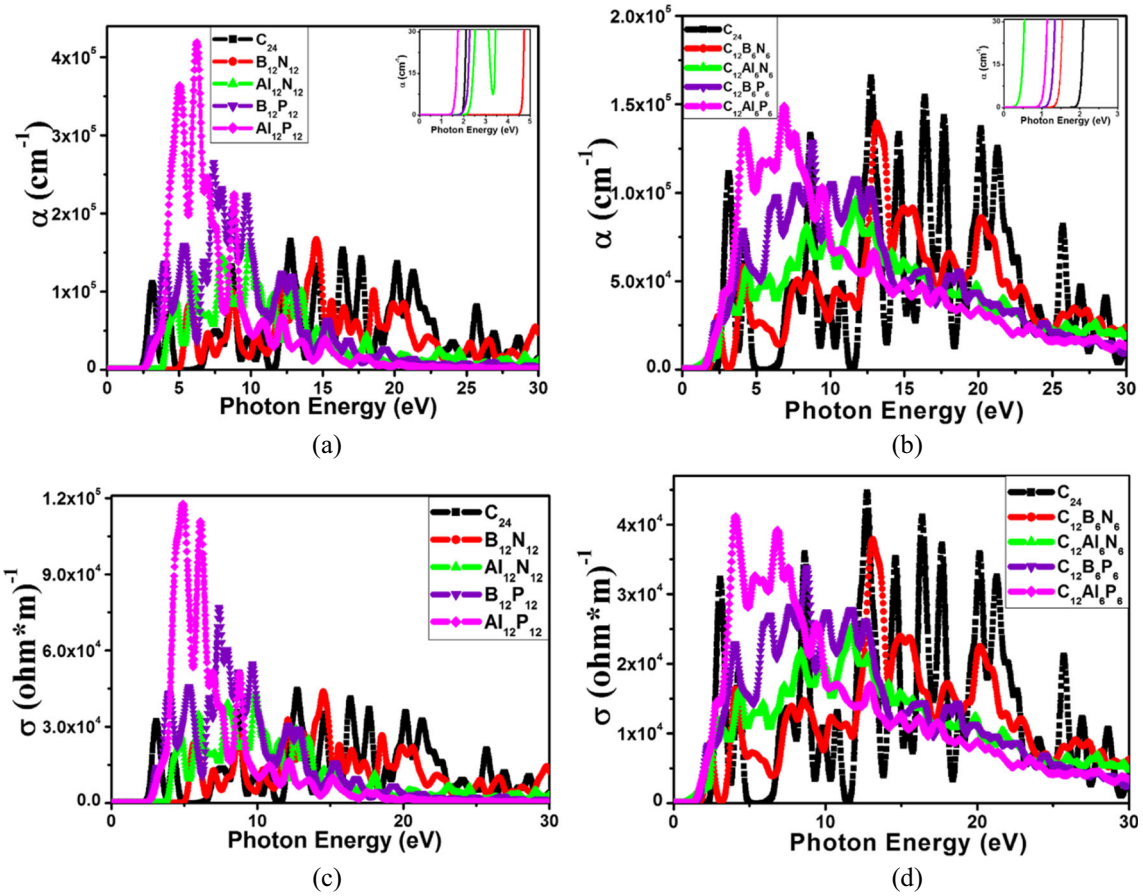

Fig. 5a–d Variations in the absorption coefficient (α; **a**, **b**) and optical conductivity (σ; **c**, **d**) with photon energy (i.e., the absorption and optical conductivity spectra) for the $X_{12}Y_{12}$ (**a**, **c**) and $C_{12}X_6Y_6$ (**b**, **d**) fullerenes

absorption for $B_{12}P_{12}$ (1.77 eV) almost overlaps with that for C_{24} (1.83 eV). All of the studied fullerenes absorb strongly in the UV region irrespective of the dopant used, which suggests that these systems could be used in UV light protection devices. The pristine fullerene shows absorption between 3 and 29 eV, and the steepest peak is located at 12.75 eV. For the $C_{12}Al_6P_6$, $C_{12}Al_6N_6$, and $C_{12}B_6P_6$ fullerenes, the primary peaks occur within the energy range 3–15 eV; outside of this range, the absorption coefficient consistently decreases. For $C_{12}B_6N_6$, the strongest peaks are distributed from 3 to 24 eV. It is apparent that the highest absorption coefficient of pristine fullerene is greater than the highest peaks of the $C_{12}X_6Y_6$ fullerenes. It can be observed that $Al_{12}P_{12}$ has the largest absorption coefficient, followed by $B_{12}P_{12}$ and then C_{24}. Upon close observation, it is clear that the highest absorption peaks for $B_{12}N_{12}$ and $Al_{12}N_{12}$ occur at 14.55 eV and 9.89 eV, respectively, similar to that of C_{24} (12.75 eV). This means that, depending upon the doping performed, there are blueshifts and redshifts of the maximum absorption coefficient of C_{24}. The optical conductivity of each system as a function of photon energy is shown in Fig. 5c, d. The optical conductivity was investigated to monitor the relative changes that occur in each system when it encounters electromagnetic radiation. Absorbing this radiation polarizes the system due to the occurrence of charge redistribution. It is worth noting that the optical conductivities of the fullerenes mimic the trend seen for their absorption coefficients, as is evident from Fig. 5. The only distinction lies in their peak amplitudes, with the peak heights in the absorption spectra exceeding the peak heights in the optical conductivity spectra.

Values of the reflectivity and the refractive index for the C_{24}, $X_{12}Y_{12}$, and $C_{12}X_6Y_6$ fullerenes are presented in Fig. 6a–d. The highest refractive index ($n_{max}(\omega)$) of the pristine fullerene occurs at an optical frequency of 2.76 eV and has a magnitude of 1.29. Among the $C_{12}X_6Y_6$ fullerenes, it is clear that $C_{12}Al_6P_6$ has the most intense refractive index peak, which is situated at 2.58 eV in the visible region, followed by $C_{12}Al_6N_6$. Among these C-containing heterofullerenes, the $n_{max}(\omega)$ values of the B-doped fullerenes occur in the visible region. Observations of the refractive index curves of $X_{12}Y_{12}$ fullerenes indicate that the $n_{max}(\omega)$ values for all of them occur in the UV region. The P-doped systems $C_{12}X_6Y_6$ and $X_{12}Y_{12}$ show the highest coefficients of $n_{max}(\omega)$. From Fig. 6a, b, it is apparent that the highest value (0.029) of the reflectivity

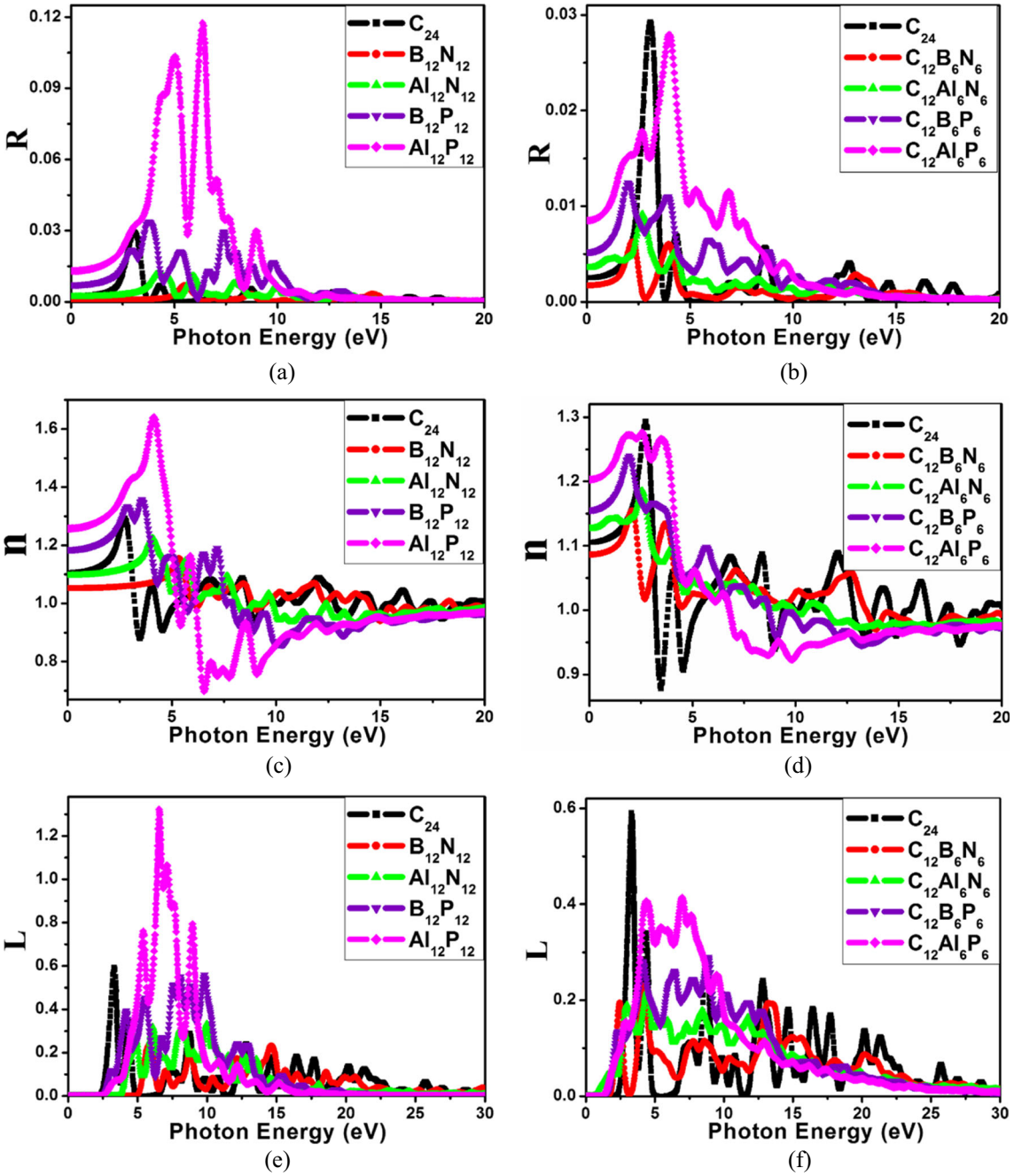

Fig. 6 Reflectivity (R), refractive index (n), and electron energy loss function (L) values of $X_{12}Y_{12}$ and $C_{12}X_6Y_6$ fullerenes

($R_{max}(\omega)$) for pristine fullerene is found at 3.09 eV, which indicates that C_{24} reflects photon, whose energy lies in the borderline of visible and UV region. All of the $C_{12}X_6Y_6$ fullerenes have lower $R_{max}(\omega)$ peak coefficients than C_{24}, and $C_{12}B_6N_6$ presents the lowest coefficient of all. As the energy increases above 13.74 eV, the reflectivity becomes almost zero, with some negligible peaks for pristine fullerene. All of the $C_{12}X_6Y_6$ fullerenes and C_{24} reflect in the visible region, except $C_{12}Al_6P_6$, which reflects in the UV region. Further, only $C_{12}Al_6P_6$ exhibits a blueshift with respect to C_{24}; redshifts are observed for other members of the $C_{12}X_6Y_6$ family. Among the $X_{12}Y_{12}$ fullerenes, $Al_{12}P_{12}$ exhibits its $R_{max}(\omega)$ (0.118) at 6.36 eV, which is higher than those of both C_{24} and the other fullerenes of this class. For the full set of fullerenes studied, the strongest reflectivity peaks occur in the UV region. $X_{12}Y_{12}$ systems show substantial reflectivity below 11.0 eV; above that, the reflectivity is trivial. Notably, the presence of N in $C_{12}X_6Y_6$ and $X_{12}Y_{12}$ results in very poor reflectivity coefficients ($C_{12}B_6N_6$ and $B_{12}N_{12}$ have the lowest coefficients in the two subgroups, respectively), as can be seen

from Fig. 6a, b. All of the fullerenes show low reflectivity values and relatively high refractive index values. These characteristics make them well suited for use in optoelectronic devices such as LEDs and solar cells.

The electron energy loss (EEL) function (L) provides a measure of the energy lost by an electron as it moves through a system. The peaks observed in the EEL spectrum relate to plasma resonance, and the corresponding frequency is known as the plasma frequency. Figure 6e, f portray the EEL spectra of $C_{12}X_6Y_6$ and $X_{12}Y_{12}$ fullerenes along with that of C_{24}. It can be seen that the prominent peaks of all the heterofullerenes, irrespective of the dopant atoms present in them, occur at energies below 15.0 eV, and the strongest peaks are blueshifted with respect to that of C_{24} towards the high-energy (UV) region. Eventually, the highest absorption peak of C_{24} as well as its doped counterparts, issituated in the UV region. It is worth noting that the $L_{max}(\omega)$ values for the doped systems are lower than that of their pristine counterpart. An exception is observed in the case of $Al_{12}P_{12}$, which has a much higher $L_{max}(\omega)$ than C_{24} does; indeed, it is the highest $L_{max}(\omega)$ value among all the fullerenes studied here. Overall, it is clear that doping causes various changes to the parameters of C_{24}, and the greatest changes are observed upon switching from C_{24} to $Al_{12}P_{12}$.

To sum up, studying the electronic and optical properties of $C_{12}X_6Y_6$ and $X_{12}Y_{12}$ (X = B, Al; Y = N, P) fullerenes affords valuable insights into the effects of introducing different dopant atoms on various properties of pristine C_{24} fullerene, as discussed above. For instance, $B_{12}N_{12}$ appears to represent an extreme case when studying electronic properties, whereas $Al_{12}P_{12}$ displays the most interesting optical properties. $B_{12}N_{12}$ shows the largest HOMO–LUMO gap, and thus the highest electrical resistivity. The DOS plot for $B_{12}N_{12}$ (Fig. 2b) indicates that its VB is dominated by contributions from N atoms, which influences the HOMO by shifting its energy states towards lower energies. B atoms contribute the most to the CB, which affects the LUMO by shifting its energy states towards higher energies. This behavior leads to a relatively wide HOMO–LUMO gap for $B_{12}N_{12}$. Also, doping with B and N leads to enhanced charge conjugation. On the other hand, the reason for the intriguing optical properties of $Al_{12}P_{12}$ is the increased charge localization caused by Al and P doping. This means that that this system shows more ionic character than fullerenes containing B and N. Further, Al and P have larger atomic radii than B and N, respectively, which means that the valence electrons of Al and P atoms are less tightly bound to their respective atomic nuclei than in the case for B and N atoms. Hence, it is clear that systems with Al and P atoms are easier to polarize than those with B and N atoms. This finding is again strongly supported by a study of the HOMO–LUMO gaps of the fullerenes of interest, which showed that $Al_{12}P_{12}$ has the smallest gap, i.e., it is the most reactive of all the $X_{12}Y_{12}$ fullerenes.

Conclusions

We have presented a detailed investigation of the electronic and optical properties of C_{24} fullerene and its doped counterparts, $C_{12}X_6Y_6$ and $X_{12}Y_{12}$ (X = B, Al; Y = N, P), using first-principles calculations. All of the systems examined were found to be thermodynamically stable according to their cohesive energy values. Calculations of their electronic properties indicated that the energy gap of C_{24} is significantly affected by doping. DOS plots implied that all of these fullerenes are semiconductors with finite energy gaps. Among all of the systems considered, $B_{12}N_{12}$ showed the highest resistivity. The redox characteristics of C_{24} could be tuned by doping this pristine system to produce heterofullerenes of formula $C_{12}X_6Y_6$, as confirmed by their lower ionization potentials than and their differences in electron affinity from $X_{12}Y_{12}$ systems, which provides the basis for exploring $C_{12}X_6Y_6$ fullerenes further. The optical properties of C_{24} and its derivatives provide useful information for future studies. All of the heterofullerenes and the pristine system presented optical gaps that make them suitable for use as optical semiconductors. In addition, the optical gap of C_{24} can be tuned from the visible region to the UV region. Given its low dielectric constant and high energy gap, $B_{12}N_{12}$ appears to be particularly applicable to use in optoelectronic devices. Upon analyzing the absorption spectra of these fullerenes, they were found to strongly absorb UV radiation, and their low reflectivity values across a wide range of energies show that these materials could potentially be used to create new optoelectronic devices such as LEDs and solar cells. Their electron energy loss spectra were also observed to be influenced by the introduction of dopants into C_{24}.

Acknowledgements US thanks ICTP, Trieste, Italy for hosting him as a regular associate. JD thanks DST, New Delhi for providing him with a DST-INSPIRE fellowship. BB thanks CSIR for providing her with a CSIR-SRF. This research is supported by Assam University, Silchar, India.

References

1. Georgakilas V, Perman JA, Tucek J, Zboril R (2015) Broad family of carbon nanoallotropes: classification, chemistry, and applications of fullerenes, carbon dots, nanotubes, graphene, nanodiamonds, and combined superstructures. Chem Rev 115:4744–4822
2. Kroto HW, Heath J, O'Brien SC, Curl RF, Smalley RE (1985) C_{60}: buckminsterfullerene. Nature 318:162–163
3. Zaghmarzi FA, Zahedi M, Mola A, Abedini S, Arshadi S, Ahmadzadeh S, Etminan N, Younesi O, Rahmanifar E, Yoosefian M (2017) Fullerene-C_{60} and crown ether doped on C_{60} sensors for high sensitive detection of alkali and alkaline earth cations. Phys E 87:51–58
4. Ross RB, Cardona CM, Guldi DM, Sankaranarayanan SG, Reese MO, Kopidakis N, Peet J, Walker B, Bazan GC, Keuren EV, Holloway BC, Drees M (2009) Endohedral fullerenes for organic photovoltaic devices. Nat Mater 8:208–212

5. Liddell PA, Kodis G, Andréasson J, de la Garza L, Bandyopadhyay S, Mitchell RH, Moore TA, Moore AL, Gust D (2004) Photonic switching of photoinduced electron transfer in a dihydropyrene−porphyrin−fullerene molecular triad. J Am Chem Soc 126:4803–4811
6. Gobbi M, Pascual A, Golmar F, Llopis R, Vavassori P, Casanova F, Hueso LE (2012) C_{60}/NiFe combination as a promising platform for molecular spintronics. Org Electron 13:366–372
7. Chen Z, Ma L, Liu Y, Chen C (2012) Applications of functionalized fullerenes in tumor theranostics. Theranostics 2:238–250
8. Orlova MA, Trofimova TP, Orlov AP, Shatalov OA (2013) Perspectives of fullerene derivatives in PDT and radiotherapy of cancers. Br J Med Med Res 3:1731–1756
9. Montellano A, Da Ros T, Bianco A, Prato M (2011) Fullerene C_{60} as a multifunctional system for drug and gene delivery. Nanoscale 3:4035–4041
10. Niu M, Yu G, Yang G, Chen W, Zhao X, Huang X (2014) Doping the alkali atom: an effective strategy to improve the electronic and nonlinear optical properties of the inorganic $Al_{12}N_{12}$ nanocage. Inorg Chem 53:349–358
11. Paul D, Deb J, Bhattacharya B, Sarkar U (2017) Density functional theory study of pristine and transition metal doped fullerene. AIP Conf Proc 1832:050107(1–3)
12. Paul D, Deb J, Bhattacharya B, Sarkar U (2017) The influence of the substitution of transition metals on pristine C_{20}: a DFT study. Int J Nanosci 16:1760026(1–5)
13. Bhusal S, Zope RR, Bhatta S, Baruah T (2016) Electronic and optical properties of $VScN@C_{68}$ fullerene. J Phys Chem C 120: 27813–27819
14. Jensen F, Toftlund H (1993) Structure and stability of C_{24} and $B_{12}N_{12}$ isomers. Chem Phys Lett 201:89–96
15. Rad AS, Ayub K (2016) A comparative density functional theory study of guanine chemisorption on $Al_{12}N_{12}$, $Al_{12}P_{12}$, $B_{12}N_{12}$, and $B_{12}P_{12}$ nanocages. J Alloys Compd 672:161–169
16. Nakamura S (1996) In: Yoshikawa A, Kishino K, Kobayashi M, Yasuda T (eds) Proceedings of international symposium on blue laser and light emitting diodes. Chiba University Press, Chiba, p 119
17. Oku T, Nishiwaki A, Narita I (2004) Formation and atomic structure of $B_{12}N_{12}$ nanocage clusters studied by mass spectrometry and cluster calculation. Sci Technol Adv Mater 5:635–638
18. Oku T, Kuno M, Kitahara H, Narita I (2001) Formation, atomic structures and properties of boron nitride and carbon nanocage fullerene materials. Int J Inorg Mater 3:597–612
19. Wu HS, Zhang FQ, Xu XH, Zhang CJ, Jiao H (2003) Geometric and energetic aspects of aluminum nitride cages. J Phys Chem A 107:204–209
20. Rad AS, Ayub K (2017) DFT study of boron trichloride adsorption on the surface of $Al_{12}N_{12}$ nanocluster. Mol Phys 115:879–884
21. Beheshtian J, Peyghan AA, Bagheri Z (2012) Quantum chemical study of fluorinated AlN nanocage. Appl Surf Sci 259:631–636
22. Ferreira V, Alves H (2008) Boron phosphide as the buffer-layer for the epitaxial III-nitride growth: a theoretical study. J Cryst Growth 310:3973–3978
23. Feng PY, Balasubramanian K (1999) Spectroscopic properties of Al_2P_2, $Al_2P_2^+$, and $Al_2P_2^-$ and comparison with their Ga and in analogues. J Phys Chem A 103:9093–9099
24. Archibong EF, Gregorius RM, Alexander SA (2000) Structures and electron detachment energies of AlP_2^- and $Al_2P_2^-$. Chem Phys Lett 321:253–261
25. Fan XF, Zhu Z, Shen ZX, Kuo J-L (2008) On the use of bond-counting rules in predicting the stability of $C_{12}B_6N_6$ fullerene. J Phys Chem C 112:15691–15696
26. Pattanayak J, Kar T, Scheiner S (2003) Comparison of BN and AlN substitution on the structure and electronic and chemical properties of C60 fullerene. J Phys Chem A 107:4056–4065
27. Bhattacharya B, Singh NB, Mondal R, Sarkar U (2015) Electronic and optical properties of pristine and boron–nitrogen doped graphyne nanotubes. Phys Chem Chem Phys 17:19325–19341
28. Bhattacharya B, Singh NB, Sarkar U (2015) Pristine and BN doped graphyne derivatives for UV light protection. Int J Quantum Chem 115:820–829
29. Ching WY, Huang MZ, Xu YN, Harter WG, Chan FT (1991) First-principles calculation of optical properties of C_{60} in the fcc lattice. Phys Rev Lett 67:2045–2048
30. Soler JM, Artacho E, Gale JD, García A, Junquera J, Ordejón P, Portal DS (2002) The SIESTA method for ab initio order-N materials simulation. J Phys Condens Matter 14:2745–2779
31. Zhai HJ, Zhao YF, Li WL, Chen Q, Bai H, Hu HS, Piazza ZA, Tian WJ, Lu HG, Wu YB, Mu YW, Wei GF, Liu ZP, Li J, Li SD, Wang LS (2014) Observation of an all-boron fullerene. Nat Chem 6:727–731
32. Chan B, Yim WL (2013) Accurate computation of cohesive energies for small to medium-sized gold clusters. J Chem Theory Comput 9:1964–1970
33. Shukla MK, Leszczynski J (2006) A density functional theory study on the effect of shape and size on the ionization potential and electron affinity of different carbon nanostructures. Chem Phys Lett 428:317–320
34. Szwacki NG, Sadrzadeh A, Yakobson BI (2007) B_{80} fullerene: an ab initio prediction of geometry, stability, and electronic structure. Phys Rev Lett 166804(1–4):98
35. Bhusal S, Rodriguez Lopez JA, Ulises Reveles J, Baruah T, Zope RR (2017) Electronic and structural study of Zn_xS_x [x= 12, 16, 24, 28, 36, 48, 96, and 108] cage structures. J Phys Chem A 121:3486–3493
36. Garg P, Kumar S, Choudhuri I, Mahata A, Pathak B (2016) Hexagonal planar CdS monolayer sheet for visible light photocatalysis. J Phys Chem C 120:7052–7060
37. Ding Y, Wang Y (2013) Density functional theory study of the silicene-like SiX and XSi_3 (X = B, C, N, Al, P) honeycomb lattices: the various buckled structures and versatile electronic properties. J Phys Chem C 117:18266–18278
38. Beheshtian J, Bagheri Z, Kamfiroozi M, Ahmadi A (2012) A comparative study on the $B_{12}N_{12}$, $Al_{12}N_{12}$, $B_{12}P_{12}$ and $Al_{12}P_{12}$ fullerene-like cages. J Mol Model 18:2653–2658
39. Ghara M, Pan S, Deb J, Kumar A, Sarkar U, Chattaraj PK (2016) A computational study on structure, stability and bonding in noble gas bound metal nitrates, sulfates and carbonates (metal = Cu, Ag, Au). J Chem Sci 10:1537–1548
40. Parr RG, Donnelly RA, Levy M, Palke WE (1978) Electronegativity: the density functional viewpoint. J Chem Phys 68:3801–3807
41. Parr RG, Pearson RG (1983) Absolute hardness: companion parameter to absolute electronegativity. J Am Chem Soc 105:7512–7516
42. Ayers PW (2007) The physical basis of the hard/soft acid/base principle. Faraday Discuss 135:161–190
43. Parr RG, Szentpály LV, Liu S (1999) Electrophilicity index. J Am Chem Soc 121:1922–1924
44. Chattaraj PK, Sarkar U, Roy DR (2006) Electrophilicity index. Chem Rev 106:2065–2091
45. Elango M, Parthasarathi R, Subramanian V, Sarkar U, Chattaraj PK (2005) Formaldehyde decomposition through profiles of global reactivity indices. J Mol Struct (THEOCHEM) 723:43–52
46. Sarkar U, Padmanabhan J, Parthasarathi R, Subramanian V, Chattaraj PK (2006) Toxicity analysis of polychlorinated dibenzofurans through global and local electrophilicities. J Mol Struct (THEOCHEM) 758:119–125
47. Chattaraj PK, Sarkar U (2003) Ground- and excited-states reactivity dynamics of hydrogen and helium atoms. Int J Quantum Chem 91: 633–650
48. Chattaraj PK, Sarkar U, Parthasarathi R, Subramanian V (2005) DFT study of some aliphatic amines using generalized philicity concept. Int J Quantum Chem 101:690–702

49. Chattaraj PK, Maiti B, Sarkar U (2003) Chemical reactivity of the compressed noble gas atoms and their reactivity dynamics during collisions with protons. J Chem Sci 115:195–218
50. Sarkar U, Khatua M, Chattaraj PK (2012) A tug-of-war between electronic excitation and confinement in a dynamical context. Phys Chem Chem Phys 14:1716–1727
51. Khatua M, Sarkar U, Chattaraj PK (2014) Reactivity dynamics of confined atoms in the presence of an external magnetic field. Eur Phys J D 68:22 **(1-9)**
52. Pearson RG (1987) Recent advances in the concept of hard and soft acids and bases. J Chem Educ 64:561–567
53. Parr RG, Chattaraj PK (1991) Principle of maximum hardness. J Am Chem Soc 113:1854–1855
54. Ayers PW, Parr RG (2000) Variational principles for describing chemical reactions: the Fukui function and chemical hardness revisited. J Am Chem Soc 122:2010–2018
55. Pegu D, Deb J, Alsenoy CV, Sarkar U (2017) Theoretical investigation of electronic, vibrational, and nonlinear optical properties of 4-fluoro-4-hydroxybenzophenone. Spectrosc Lett 50:232–243
56. Saha SK, Deb J, Sarkar U, Paul MK (2017) Hockey-stick-shaped mesogens based on 1,3,4-thiadiazole: synthesis, mesomorphism, photophysical and DFT studies. Liq Cryst 44:2203–2221
57. Chamorro E, Chattaraj PK, Fuentealba P (2003) Variation of the electrophilicity index along the reaction path. J Phys Chem A 107: 7068–7072
58. Yang L-M, Ravindran P, Vajeeston P, Tilset M (2012) Properties of IRMOF-14 and its analogues M-IRMOF-14 (M = Cd, alkaline earth metals): electronic structure, structural stability, chemical bonding, and optical properties. Phys Chem Chem Phys 14:4713–4723
59. Yang L-M, Ravindran P, Vajeeston P, Tilset M (2012) Ab initio investigations on the crystal structure, formation enthalpy, electronic structure, chemical bonding, and optical properties of experimentally synthesized isoreticular metal-organic framework-10 and its analogues:*M*-IRMOF-10 (*M* = Zn, Cd, Be, Mg, Ca, Sr and Ba). RSC Adv 2:1618–1631
60. Paul D, Bhattacharya B, Deb J, Sarkar U (2018) Optical properties of C_{28} fullerene cage: a DFT study. AIP Conf Proc 1953: 030236(1–3)
61. Bhattacharya B, Sarkar U (2016) The effect of boron and nitrogen doping in electronic, magnetic, and optical properties of graphyne. J Phys Chem C 120:26793–26806